PNAS RESEARCH ARTICLE | MICROBIOLOGY

Bacterial SEAL domains undergo autoproteolysis and function in regulated intramembrane proteolysis

Anna P. Brogan[a], Cameron Habib[a], Samuel J. Hobbs[a,b], Philip J. Kranzusch[a,b], and David Z. Rudner[a,1]

Edited by Susan Gottesman, National Cancer Institute, Bethesda, MD; received June 27, 2023; accepted August 25, 2023

Gram-positive bacteria use SigI/RsgI-family sigma factor/anti-sigma factor pairs to sense and respond to cell wall defects and plant polysaccharides. In *Bacillus subtilis,* this signal transduction pathway involves regulated intramembrane proteolysis (RIP) of the membrane-anchored anti-sigma factor RsgI. However, unlike most RIP signaling pathways, site-1 cleavage of RsgI on the extracytoplasmic side of the membrane is constitutive and the cleavage products remain stably associated, preventing intramembrane proteolysis. The regulated step in this pathway is their dissociation, which is hypothesized to involve mechanical force. Release of the ectodomain enables intramembrane cleavage by the RasP site-2 protease and activation of SigI. The constitutive site-1 protease has not been identified for any RsgI homolog. Here, we report that RsgI's extracytoplasmic domain has structural and functional similarities to eukaryotic SEA domains that undergo autoproteolysis and have been implicated in mechanotransduction. We show that site-1 proteolysis in *B. subtilis* and Clostridial RsgI family members is mediated by enzyme-independent autoproteolysis of these SEA-like domains. Importantly, the site of proteolysis enables retention of the ectodomain through an undisrupted β-sheet that spans the two cleavage products. Autoproteolysis can be abrogated by relief of conformational strain in the scissile loop, in a mechanism analogous to eukaryotic SEA domains. Collectively, our data support the model that RsgI–SigI signaling is mediated by mechanotransduction in a manner that has striking parallels with eukaryotic mechanotransducive signaling pathways.

autoproteolysis | SEA domain | mechanotransduction | regulated intramembrane proteolysis

Mechanotransduction is an emerging mode of signal transduction in which cells sense and respond to force stimuli. Well-characterized examples include adhesion G protein–coupled receptors (aGPCRs) and Notch receptors (1–3). In the case of aGPCRs, the extracellular domains of these receptors bind the extracellular matrix or surface ligands on a neighboring cell and shear force triggers aGPCR signaling. Similarly, Notch receptors bind membrane-anchored ligands on signal-sending cells. Endocytosis of the ligand-bound complex by the signal-sending cell generates a pulling force that activates Notch in the signal-receiving cell. In these and other examples, proteolysis plays a central role in mechanotransduction. aGPCRs undergo autoproteolysis in their extracellular domain but the cleaved fragments remain noncovalently associated. Mechanical force is hypothesized to pull the fragments apart revealing a membrane-tethered agonist that triggers G-protein Coupled Receptor (GPCR) signaling. In the case of Notch, the mechanical force exerted on its extracellular domain causes a conformational change that reveals a cleavage site for a membrane-anchored protease. Ectodomain cleavage and release triggers intramembrane proteolysis by gamma-secretase and information transduction. Thus, this regulated intramembrane proteolysis (RIP) pathway is activated by mechanical force. In contrast to these well-characterized eukaryotic systems, there are very few examples of bacterial mechanotransducive pathways and those that have been identified remain poorly understood. Our recent work on how the bacterium *Bacillus subtilis* responds to cell wall defects has uncovered a signaling pathway (4) that appears to combine features of aGPCR and Notch signaling.

Regulated intramembrane proteolysis (RIP) is a broadly conserved mechanism of information transduction that involves a two-step proteolytic pathway (5). In bacteria, the principal targets of RIP signaling are membrane-anchored anti-sigma factors that hold their cognate sigma factors inactive (6). External stimuli trigger "site-1" cleavage of the anti-sigma factor on the extracytoplasmic side of the membrane. A diverse set of bacterial proteases have been implicated in this regulated step. Ectodomain release allows the membrane-anchored portion of the anti-sigma factor access to the recessed interior of the S2P/RseP family of membrane-embedded "site-2" proteases (7, 8). Site-2 cleavage leads to release of the sigma factor and activation of gene expression. The *B. subtilis* RsgI anti-sigma factor is subject to RIP in response to cell wall defects (9) but unlike previously characterized bacterial RIP pathways, the activating step is not site-1 cleavage. In this

Significance

SEA domains are broadly conserved among eukaryotes but absent in bacteria. They are present on diverse membrane-anchored proteins some of which have been implicated in mechanotransducive signaling pathways. Many of these domains have been found to undergo autoproteolysis and remain noncovalently associated following cleavage. Their dissociation requires mechanical force. Here, we identify a family of bacterial SEA-like domains that arose independently from their eukaryotic counterparts but have structural and functional similarities. We show that these domains autocleave and the cleavage products remain associated. SEAL domains are present on membrane-anchored anti-sigma factors that have been implicated in mechanotransduction pathways. Our findings suggest that bacterial and eukaryotic signaling systems have evolved a similar mechanism to transduce mechanical stimuli across the lipid bilayer.

Author contributions: A.P.B. and D.Z.R. designed research; A.P.B. performed research; A.P.B., C.H., and S.J.H. contributed new reagents/analytic tools; A.P.B., S.J.H., P.J.K., and D.Z.R. analyzed data; C.H., S.J.H., and P.J.K. edited manuscript; and A.P.B. and D.Z.R. wrote the paper.

The authors declare no competing interest.

This article is a PNAS Direct Submission.

[1]To whom correspondence may be addressed. Email: rudner@hms.harvard.edu.

This article contains supporting information online at https://www.pnas.org/lookup/suppl/doi:10.1073/pnas.2310862120/-/DCSupplemental.

Published September 27, 2023.

noncanonical RIP signaling pathway, site-1 cleavage appears to be constitutive but the two cleavage products remain associated. Activation of intramembrane proteolysis is mediated by their dissociation, which is hypothesized to involve a signal that generates mechanical force (4). Site-2 cleavage of RsgI releases the cognate sigma factor SigI that, in turn, activates genes involved in peptidoglycan (PG) biogenesis (10–12).

Here, we report that the extracytoplasmic domain of RsgI has structural and functional similarities to eukaryotic sea urchin sperm protein, enterokinase, agrin (SEA) domains (13). Intriguingly, many eukaryotic SEA domains undergo autoproteolysis and a subset have been implicated in mechanotransduction (14–17). We show that site-1 cleavage of *B. subtilis* RsgI and Clostridial homologs is mediated by enzyme-independent autoproteolysis in these SEA-like (SEAL) domains. Importantly, the site of proteolysis enables retention of the ectodomain through an undisrupted β-sheet that spans the two cleavage products, similar to what has been observed for aGPCRs (18). Furthermore, we show that autoproteolysis can be abrogated by relief of conformational strain in the scissile loop, in a mechanism analogous to eukaryotic SEA domains (19, 20). Intriguingly, SEAL domains are present throughout Firmicutes where they are fused to anti-sigma factors as well as diverse extracytoplasmic domains. We demonstrate that several of these SEAL domains also undergo autoproteolysis at a conserved site and the cleaved fragments remain stably associated. Collectively, our data define a family of bacterial SEAL domains that arose independently from their eukaryotic counterparts and argue that RsgI–SigI signaling is mediated by mechanotransduction in a manner that is similar to eukaryotic mechanotransducive signaling systems.

Results

The AlphaFold Model of RsgI's Juxtamembrane Domain Is Structurally Similar to SEA Domains. Previous genetic screens in *B. subtilis* that implicated the S2P/RseP family member RasP in the SigI–RsgI signaling pathway failed to identify a site-1 protease (4, 9). Attempts to identify this protease using targeted disruption of known secreted and membrane-anchored extracytoplasmic proteases were unsuccessful. Instead, our analysis of the AlphaFold2-predicted structure (21) of RsgI led us to find that constitutive site-1 proteolysis is mediated by autoproteolysis. The predicted structure of RsgI contains an N-terminal cytoplasmic anti-sigma factor domain, a transmembrane segment, and an extracytoplasmic juxtamembrane domain (JMD) followed by a long intrinsically disordered region (IDR) (Fig. 1*A*). The RsgI model has a relatively high confidence with an overall average predicted local distance difference test (pLDDT) of 72.97. However, it has a very high average pLDDT (94.16) within the folded JMD (*SI Appendix*, Fig. S1). We have previously shown that site-1 cleavage occurs within the JMD and that the IDR is important for signaling and could be responsible for the mechanical force that dissociates the site-1 cleavage products (4). To investigate potential mechanisms of site-1 proteolysis and ectodomain retention, we used the high-confidence model to search for structural homologs of the JMD in the Protein Data Bank.

The top hit using the DALI server (22) was an N-terminal asparagine amidohydrolase that had modest structural similarity to RsgI's JMD. Several other top hits were also enzymes, but none of their active sites aligned well with RsgI (*SI Appendix*, Table S1). These findings prompted us to consider that RsgI's JMD could have enzymatic activity. Specifically, we wondered whether this domain undergoes autoproteolysis. In reading about extracytoplasmic autoproteases, we noticed that the AlphaFold2 model of RsgI's JMD had a similar fold to eukaryotic sea urchin sperm protein, enterokinase, agrin (SEA) domains (17, 23). SEA domains are broadly conserved among eukaryotes but homologs have not been identified in bacteria. Several of these domains have been shown to undergo autoproteolysis and remain noncovalently associated following cleavage. Furthermore, some have been implicated in mechanotransduction. Although SEA domains were not identified as structurally similar to RsgI's JMD using the DALI server, both consist of alternating α-helices and β-strands that form a β-sheet packed at its concave face against two α-helices (Fig. 1 *A*–*C*). A structural alignment using TM-align (24) of RsgI's JMD with the predicted structure of the most well-studied SEA domain, *Homo sapiens* Mucin-1 (MUC1), revealed a rmsd of 4.82 Å over 75 amino

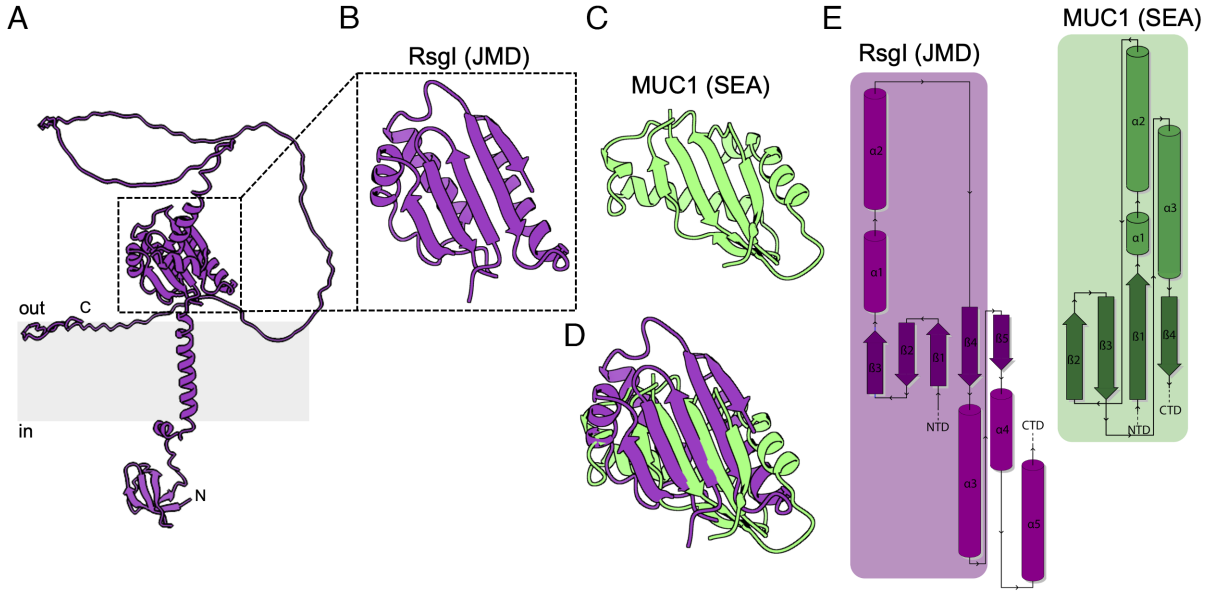

Fig. 1. The Alphafold2-predicted structure of RsgI's juxtamembrane domain has structural similarity to eukaryotic SEA domains. (*A*) AlphaFold2-predicted model of *B. subtilis* RsgI. The membrane bilayer is shown in gray. (*B*) Zoom-in of the juxtamembrane domain (JMD). (*C*) Crystal structure of the SEA domain from *H. sapiens* Mucin-1 (MUC1) (pdb: 6bsb). (*D*) Structural alignment by TM-align of the AlphaFold2-predicted structure of RsgI's JMD and the crystal structure of MUC1's SEA domain. (*E*) Protein topology maps of RsgI's JMD and the SEA domain in MUC1 as generated by PDBsum.

acids, and a TM-align score of 0.35, further suggesting that the domains are unlikely to be homologous (*SI Appendix*, Fig. S2). Furthermore, RsgI's JMD and the MUC1 SEA domain contain similar secondary structural elements but their interconnectivities are distinct (Fig. 1*D*). Thus, the JMD and SEA domains likely evolved convergently to adopt a similar fold. Based on the experiments presented below, we have named RsgI's JMD a SEAL domain for SEA-like.

***B. subtilis* RsgI Undergoes Autoproteolysis.** Many SEA domains undergo autoproteolysis at a conserved site in a β-hairpin and remain noncovalently associated following cleavage (14, 15, 25) Although RsgI's SEAL domain lacks the autoproteolytic site found in SEA domains, we investigated whether it undergoes autoproteolysis. We fused the soluble SEAL domain to an N-terminal His-SUMO tag and expressed it in *Escherichia coli* followed by Ni^{2+}-affinity chromatography. The purification yielded three polypeptides of ~35, 15, and 14 kDa (Fig. 2*A*). Mass spectrometry revealed that the 35 kDa species was the full-length His-SUMO-SEAL fusion. The two smaller polypeptides corresponded to the N- and C-terminal fragments derived from cleavage within the SEAL domain. Importantly, incubation of the purified proteins at 37 °C resulted in further loss of the full-length protein and accumulation of the cleaved products (Fig. 2*B*), consistent with autocleavage. However, to exclude the possibility that a contaminating *E. coli* protease was responsible for the observed proteolysis, we performed protease-free in vitro transcription–translation reactions using ^{35}S-methinonine and a *gfp-rsgI(SEAL)* gene fusion as a template. After a 60 min reaction, we observed full-length Green Fluorescent Protein (GFP)-SEAL and two cleavage products (Fig. 2*C*). Inhibition of protein synthesis with chloramphenicol at 60 min resulted in further loss of the full-length species. Taken together, these data suggest that *B. subtilis* RsgI's SEAL domain is an autoprotease.

Autoproteolysis Is a Conserved Feature among RsgI Homologs. Many Clostridial species encode SigI/RsgI homologs and several of these have been found to regulate the expression of genes involved in the degradation of cellulose and other plant cell wall polysaccharides (26–29). The genes encoding cellulolytic enzymes are induced in the presence of these large polysaccharides that are unable to cross the bacterial cell wall. Several Clostridial RsgI homologs have carbohydrate-binding modules (CBMs) appended to their IDRs and we previously proposed that cellulose binding to these domains generates a pulling force that could dissociate the site-1-cleaved products (Fig. 3*A*) (4). However, it was unknown whether these RsgIs are cleaved by a site-1 protease. Prompted by our finding that *B. subtilis* RsgI is an autoprotease, we investigated whether Clostridial RsgI homologs also undergo autoproteolysis. We expressed and purified His-SUMO-fusions to the SEAL domains of RsgI from *Clostridium thermoalcaliphilum* and RsgI2 and RsgI4 from *Hungateiclostridium thermocellum*. All three purifications contained cleavage products and a small amount of full-length protein (Fig. 3*B*). Similar to *B. subtilis* RsgI's SEAL domain, the full-length *C. thermoalcaliphilum* His-SUMO-SEAL fusion was further lost during incubation at 37 °C (Fig. 3*C*). These data argue that the SEAL domains of Clostridial RsgI homologs undergo autoproteolysis and provide support for the model that plant polysaccharides trigger SigI activation via mechanotransduction (Fig. 3*A*). A recent report provides strong support for this model and implicates the *H. thermocellum* RasP homolog as the site-2 protease (30).

To identify the cleavage site within the SEAL domains, we performed Edman degradation on the C-terminal cleavage products (Fig. 3*D*). For all SEAL domains analyzed, the cleavage site mapped between N97 and P98 (Fig. 3*E* and *SI Appendix*, Fig. S3). The cleavage site was independently confirmed by top–down (intact) mass spectrometry using MALDI-TOF (*SI Appendix*, Fig. S4). Importantly, our previous mass spectrometry analysis of the in vivo cleavage products of *B. subtilis* RsgI is consistent with site-1 cleavage occurring at this exact position (*SI Appendix*, Fig. S5). The cleavage site lies in a conserved three amino acid β-hairpin between two β-strands in the predicted structures (Fig. 3*F*). Importantly, cleavage is predicted to leave the β-sheet intact and thereby allow ectodomain retention. This cleavage site is analogous to the cleavage site in the MUC1 SEA domain, which also lies in a β-hairpin (15, 31), although there is no amino acid conservation between them (Fig. 3*F*).

RsgI Autoproteolysis Is Catalyzed by Conformational Strain. Autoproteolysis of eukaryotic SEA domains is largely driven by conformational strain in the scissile β-hairpin (15, 19, 20). In particular, amino acid substitutions of the nucleophilic residue in MUC1 impair but do not abrogate cleavage (32). Rather, insertion of glycine residues adjacent to the cleavage site to relax the torsional strain strongly impairs cleavage (23, 33). Our attempts to block autoproteolysis of RsgI's SEAL domain by substituting conserved

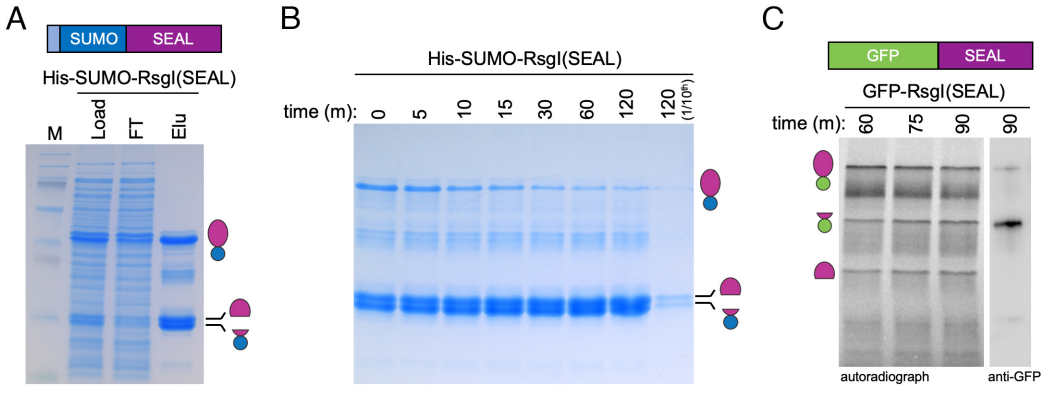

Fig. 2. RsgI's SEAL domain undergoes autoproteolysis. (*A*) Coomassie-stained SDS-PAGE gel of His-SUMO-RsgI(SEAL) expressed and purified from *E. coli*. His-SUMO-RsgI(SEAL) was expressed for 3 h, and the clarified lysate (Load) was subjected to affinity chromatography. The flowthrough (FT) was collected and His-SUMO-RsgI(SEAL) eluted (Elu) by the addition of imidazole. Full-length His-SUMO-RsgI(SEAL) and cleaved products are indicated. (*B*) Coomassie-stained gel of the elution in (*A*) at the indicated times (in min) after incubation at 37 °C. (*C*) Autoradiograph and immunoblot of an in vitro transcription–translation reaction with ^{35}S-methionine using *gfp-rsgI(SEAL)* as a template. Chloramphenicol was added 60 min after the reaction was initiated to inhibit protein synthesis. Note that 75- and 90-min timepoints have an increase in cleavage products and a reduction in full-length protein. Anti-GFP immunoblot is from the 90-min reaction diluted 1:50. The purification, timecourse, and in vitro transcription–translation reaction were performed in biological triplicate, and representative gels are shown.

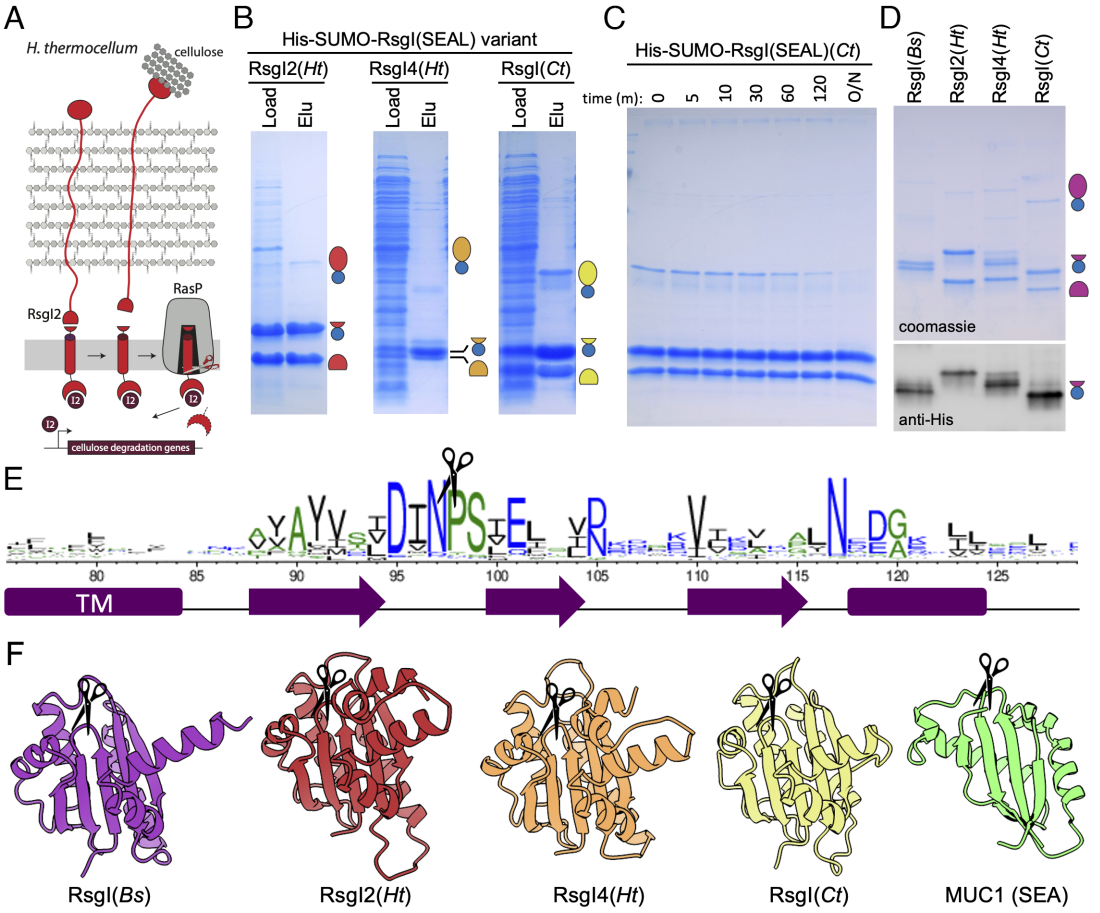

Fig. 3. RsgI homologs undergo autoproteolysis at a conserved cleavage site. (*A*) Schematic model of the RsgI2-Sig2 signal transduction pathway in *H. thermocellum*. Cellulose binding to the carbohydrate-binding module on RsgI2 generates a pulling force that dissociates the cleaved SEAL domain and enables RasP-mediated intramembrane proteolysis. Release of SigI2 (I2) activates genes involved in cellulose degradation. (*B*) Coomassie-stained gels of His-SUMO-RsgI(SEAL) fusions from *H. thermocellum* (*Ht*) RsgI2 and RsgI4 and *C. thermoalcaliphilum* (*Ct*) RsgI. Load and elution (Elu) are shown. All purifications were performed in biological triplicate, and a representative gel is shown. (*C*) Coomassie-stained gel of purified His-SUMO-RsgI(SEAL) (*Ct*) after incubation at 37 °C for the indicated times. (*D*) Coomassie-stained gel and immunoblot of purified His-SUMO-RsgI(SEAL) variants. Purified proteins were diluted 1:50 for the immunoblot. (*E*) Sequence logo determined from the alignment of >5,000 RsgI homologs. Adapted from Brunet et al. (4). The autocleavage site is highlighted (scissors). (*F*) AlphaFold2-predicted structures of SEAL domains from RsgI homologs with their cleavage sites (scissor) indicated. The crystal structure and cleavage site of MUC1's SEA domain are included for comparison.

amino acids proximal to the cleavage site similarly slowed but did not abolish cleavage (*SI Appendix*, Fig. S6*A*). Given the structural and functional similarities between the SEAL and SEA domains, we investigated whether relaxing the strain within the scissile loop of RsgI's SEAL domain would abrogate cleavage. We inserted three glycine residues adjacent to the cleavage site (between I96 and N97) and purified the mutant from *E. coli* (Fig. 4*A*). Strikingly, purified His-SUMO-SEAL^{GGG} was almost entirely full-length (Fig. 4*B*). Furthermore, we detected no loss of the full-length product after incubation of the purified protein at 37 °C for >10 h (Fig. 4*C* and *SI Appendix*, Fig. S6*B*). Finally, a protease-free in vitro transcription–translation reaction using *gfp-rsgI(SEAL^{GGG})* as a template produced only the full-length product (Fig. 4*D*). Collectively, these data indicate that autoproteolysis of RsgI is catalyzed by conformational strain.

Crystal Structure of the SEAL^{GGG} Domain. To experimentally determine the structure of the SEAL domain, we took advantage of the stability of the SEAL^{GGG} variant. The His-SUMO-SEAL^{GGG} fusion was affinity purified and, following removal of the His-SUMO tag, further purified by size-exclusion chromatography. Crystals were raised via hanging drop vapor diffusion and the structure of the SEAL^{GGG} domain was determined at 1.9 Å resolution (Fig. 4*E*). The structure revealed a fold consisting of five β-strands that form a β-sheet packed against two α-helices occurring in the order β1-β2-β3-α1-α2-β4-α3-β5-α4-α5, with α4 and α5 only resolved on one of the two molecules in the asymmetric unit. The entire experimentally determined SEAL^{GGG} structure was nearly superimposable on the AlphaFold2 model with a rmsd of 1.08 Å and a TM-align score of 0.97 (*SI Appendix*, Fig. S7). The electron density in the glycine loop region was weak, suggesting that the loop is highly flexible and may consist of a mixture of cleaved and uncleaved species (*SI Appendix*, Fig. S8). For simplicity, we have modeled it as the uncleaved variant in Fig. 4*E*.

Interestingly, β1 and β2, which surround the β-hairpin cleavage site, had extended β-strands in the crystal structure compared to the AlphaFold2 prediction of the wild-type SEAL domain (*SI Appendix*, Fig. S9). Specifically, I96 and P101 of the β-hairpin are incorporated into β1 and β2, respectively, and the inserted glycine residues largely populate the β-turn (*SI Appendix*, Fig. S9). Notably, both the AlphaFold2 prediction of the SEAL^{GGG} variant and the AlphaFold-multimer prediction of the cleavage products predict a similar β-strand-extension and provide a mechanism of strain relief in the loop (*SI Appendix*, Fig. S9). Previous studies on SEA domains have shown that the short β-hairpin turn precludes proper folding in the absence of autoproteolysis (23). Our structure suggests that the mechanism of strain-catalyzed cleavage is likely to be conserved between SEA and SEAL domains.

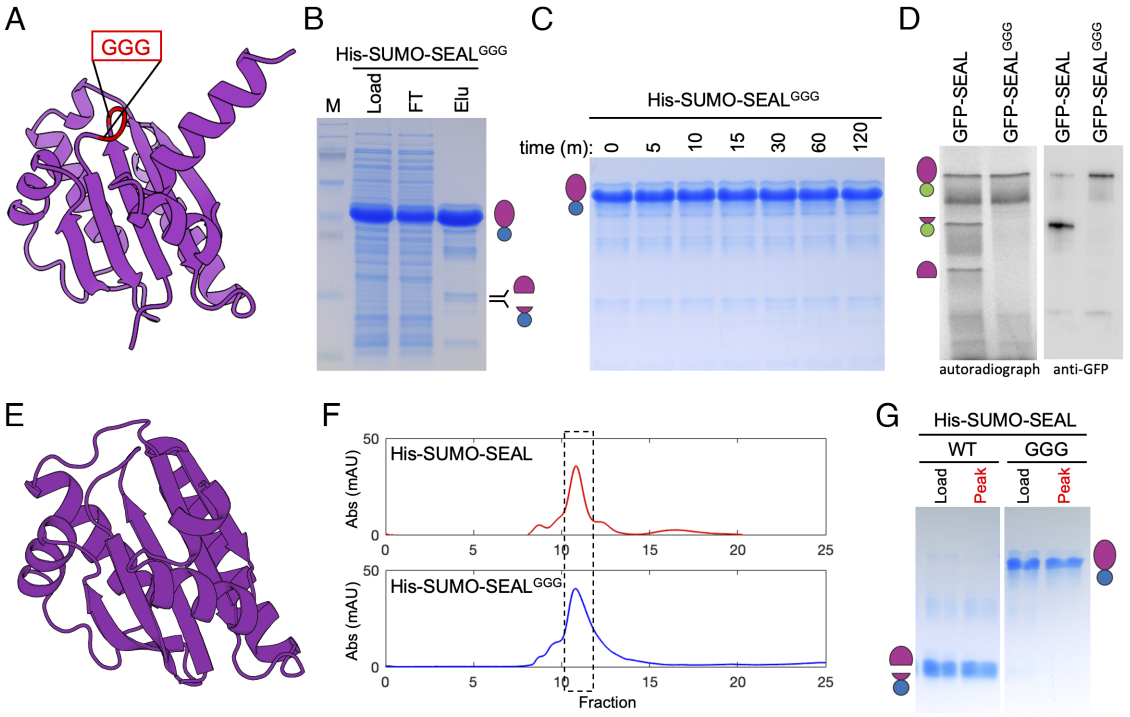

Fig. 4. Autoproteolysis of RsgI's SEAL domain is catalyzed by conformational strain. (*A*) AlphaFold2 model of SEAL^{GGG} with the inserted glycines in red. (*B*) Coomassie-stained gel of His-SUMO-SEAL^{GGG} expressed and purified from *E. coli*. Load, flowthrough (FT), and eluate (Elu) from Ni^{2+}-affinity chromatography are shown. (*C*) Coomassie-stained gel of purified His-SUMO-SEAL^{GGG} after incubation at 37 °C for the indicated times in min. (*D*) Autoradiograph and immunoblot showing GFP-SEAL and GGG variant after a 90-min in vitro transcription–translation reaction with ^{35}S-methionine. Reactions were diluted 1:100 for visualization by immunoblot. (*E*) Cartoon rendering of the crystal structure of the *B. subtilis* SEAL^{GGG} domain. (*F*) Size-exclusion chromatograms for purified His-SUMO-SEAL and His-SUMO-SEAL^{GGG}. (*G*) SDS-PAGE gel of the peak fraction (boxed in red) compared to load. The purification, timecourse, and in vitro transcription–translation reaction were performed in biological triplicate, and representative gels are shown.

RsgI's Autoproteolytic Products Remain Stably Associated. In both the SEAL^{GGG} structure and AlphaFold-multimer prediction of the site-1 cleavage products, the two β-strands bridged by the β-hairpin are extended after cleavage creating additional hydrogen bond contacts between them. In the context of SEAL domain autoproteolysis, the extended β-strands would likely further stabilize the interaction between the two cleavage products. We note that the Ni^{2+}-affinity purification of the His-SUMO-SEAL fusions contained both cleavage products even though only one of the two contained a His tag. This strongly suggests that the cleaved products remain stably associated through the hydrogen bond network in the β-sheet. However, it was formally possible that the full-length His-SUMO-SEAL fusion autoproteolyzed during elution and the two products do not interact. To distinguish between these models, we performed analytical size exclusion chromatography on purified His-SUMO-SEAL and the GGG variant. As can be seen in Fig. 4*F*, the peak fractions and overall traces were similar. Importantly, the peak fraction from the SEAL domain contained the two cleavage products while SEAL^{GGG} was full-length (Fig. 4*G*). We conclude that RsgI remains noncovalently associated after autoproteolysis.

RsgI^{GGG} Abrogates Site-1 Cleavage In Vivo. To investigate whether RsgI undergoes autoproteolysis in vivo, we generated the triple-glycine mutant in the full-length protein. To visualize the RsgI cleavage products, we used a previously characterized variant with GFP fused to the N terminus and a His-tag at the C-terminus (4). Exponentially growing *B. subtilis* cells expressing GFP-RsgI-His or the GGG mutant were harvested before and at time points after inhibition of translation to monitor the fate of RsgI and its cleavage products. As reported previously, only a minor fraction of wild-type RsgI was full-length and both the N- and C-terminal site-1 cleavage products were readily detectable (Fig. 5*A*) (4). The N-terminal site-2 cleaved product was also observed. Furthermore, the cleavage products were largely stable after inhibition of protein synthesis. By contrast, most of the RsgI^{GGG} variant was full-length with a small amount of site-1 cleaved fragments (Fig. 5*A*), similar to what was observed in vitro (Fig. 4*B*). We conclude that RsgI undergoes autoproteolysis in vivo and is responsible for the constitutive site-1 cleavage in this RIP signaling pathway.

We have previously shown that the two site-1 cleavage products are rapidly lost in cells lacking the major cell wall synthase PBP1 (Fig. 5*A*) (4). The N-terminal membrane fragment is cleaved by the membrane-embedded site-2 protease RasP leading to SigI activation, while the C-terminal fragment is degraded probably upon release into the medium. Importantly, SigI activation and loss of the two cleavage products do not occur if RsgI lacks its intrinsically disordered region (IDR) (4). These results led to the hypothesis that the IDR senses cell wall defects and generates a mechanical force that pulls the cleavage products apart, enabling intramembrane proteolysis and SigI activation. To investigate whether the RsgI^{GGG} variant is able to respond to cell wall stress, we analyzed the mutant in cells lacking PBP1. Surprisingly, the full-length RsgI^{GGG} protein was rapidly lost and the site-2 cleavage product was readily detectable (Fig. 5*A*). Furthermore, analysis of SigI activity using a SigI-responsive promoter (P*bcrC*) fused to *lacZ* (4) revealed that wild-type RsgI and the RsgI^{GGG} variant activate SigI similarly in the absence of PBP1 or after inhibition of its activity (Fig. 5*B* and *SI Appendix*, Fig. S10*A*). These data indicate that intramembrane proteolysis and SigI activation can occur in response to cell wall defects independently of site-1 autoproteolysis.

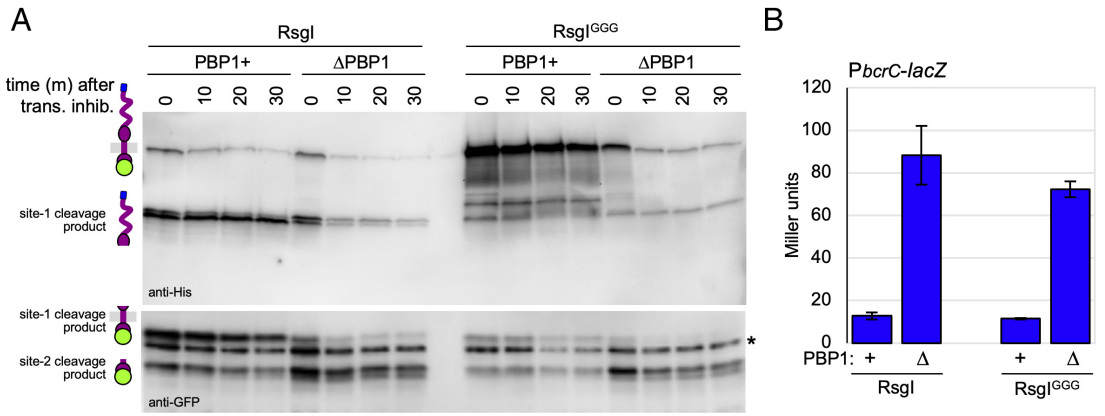

Fig. 5. RsgI autoproteolysis occurs in vivo but is not required for SigI signaling. (*A*) Immunoblot of *B. subtilis* cells constitutively expressing GFP-RsgI-His or GFP-RsgI^{GGG}-His in the indicated backgrounds. Timepoints (in minutes) before and after treatment with chloramphenicol and spectinomycin to inhibit protein synthesis are shown. Full-length GFP-RsgI^{GGG}-His accumulates in cells with intact cell walls (PBP1+) but not in the ΔPBP1 mutant. A cross-reactive band in the anti-GFP immunoblot is indicated with an asterisk (*). The blot was performed in biological triplicate, and a representative blot is shown. (*B*) Bar graph showing β-galactosidase activity of a SigI-responsive (P_{bcrC}) reporter. Strains harboring untagged RsgI and RsgI^{GGG} respond similarly to cell wall defects (ΔPBP1). All β-galactosidase assays were performed in biological triplicate, and error bars indicate SE among these.

Intramembrane Proteolysis in the Absence of Site-1 Cleavage Requires RsgI's IDR. Our findings suggest that autoproteolysis occurs in vivo but preventing it is not sufficient to block intramembrane proteolysis and activation of SigI. One model that could explain these results is that the force required to dissociate the site-1-cleaved products is similar to the force required to partially or completely unfold the SEAL domain and, once unfolded, it is cleaved by an unknown extracytoplasmic protease and/or becomes accessible to the membrane-embedded site-2 protease (Fig. 6*A*).

Previous studies indicate that the IDR is required to dissociate the cleaved products enabling intramembrane proteolysis and SigI activation (4). To investigate whether the IDR was still required to trigger intramembrane proteolysis when site-1 cleavage was blocked, we analyzed the RsgI^{GGG} variant lacking its IDR. As can be seen in Fig. 6*B*, the RsgI^{GGG}ΔIDR mutant remained full-length in the presence *and* absence of PBP1. Similarly, activation of SigI is blocked in the RsgI^{GGG}ΔIDR mutant (*SI Appendix*, Fig. S10*B*). This suggests that the predicted mechanical force imparted by the IDR is required for signaling and that this force could drive unfolding of the SEAL domain.

To investigate whether RsgI^{GGG} was cleaved by an extracytoplasmic protease prior to intramembrane proteolysis or was directly processed by the site-2 protease RasP, we analyzed the mutant in cells lacking RasP. For these experiments, we used *rasP*$^{+}$ and Δ*rasP* strains. However, cells lacking RasP and PBP1 are not viable (4, 9). Accordingly, to generate cell wall defects to trigger signaling, we inhibited the glycosyltransferase activity of PBP1 using the drug moenomycin (34) prior to analyzing RsgI^{GGG}. In the presence of the membrane-embedded protease RasP and moenomycin, full-length RsgI^{GGG} was efficiently cleaved by the site-2 protease similar to cells lacking PBP1 (Fig. 6*C*). In the absence of RasP, loss of the full-length product was slower but a membrane-anchored RsgI fragment similar in size to the N-terminal fragment of autoproteolyzed RsgI accumulated. These data are consistent with a model in which partial or complete unfolding of the juxtamembrane domain in response to cell wall stress leads to cleavage by an extracytoplasmic protease that enables intramembrane proteolysis by RasP. This layered proteolysis is not unprecedented in mechanotransducive systems and is reminiscent of Notch signaling, in which a pulling force generates a conformational change in its ectodomain that enables cleavage by an extracellular protease that triggers intramembrane proteolysis (35). However, we note that cleavage of RsgI^{GGG} by this unknown extracytoplasmic protease was slower in the absence of RasP, suggesting that RasP could be partially responsible for the direct processing of RsgI^{GGG} without prior proteolytic processing. Thus, our data suggest that partial or complete unfolding of the SEAL domain in response to cell wall defects enables cleavage by an extracytoplasmic site-1 protease but also may allow RasP-mediated intramembrane proteolysis without ectodomain cleavage and release.

Discussion

Recent studies on the RsgI–SigI signaling system in *B. subtilis* revealed that RsgI is subject to regulated intramembrane proteolysis in response to cell wall defects (4, 9, 36). Analysis of the RsgI cleavage products in unperturbed cells strongly suggested that, unlike canonical RIP signaling pathways, site-1 cleavage is constitutive. The regulated step in this pathway was hypothesized to be the dissociation of the site-1 cleavage products by a mechanical force generated by RsgI's intrinsically disordered region upon encountering cell wall defects. Here, we show that constitutive site-1 cleavage of RsgI is mediated by autoproteolysis and that the cleavage products remain stably associated, analogous to eukaryotic SEA domains. These data bolster the proposed model for RsgI–SigI signaling and provide support for the role of mechanical force in the activation of intramembrane proteolysis. Although the mechanism of force generation remains unclear in *B. subtilis*, our analysis of the Clostridial RsgIs suggests a clearly defined pulling force in the activation of their cognate sigma factors. Since cellulose and related carbohydrates are too large to enter the PG meshwork, it has been proposed that the IDRs on Clostridial RsgIs span the envelope layers displaying their carbohydrate-binding modules on the cell surface (26, 27). Cellulose bound to these domains could generate a shear force that would dissociate the SEAL domain autocleavage products and trigger intramembrane proteolysis (Fig. 3*A*). Importantly, these Clostridial species encode RasP homologs, suggesting that their RsgI homologs are subject to RIP signaling. Collectively, our data lead us to propose that homologous SigI–RsgI signaling systems sense and respond to a broad array of extracellular macromolecules using the same mechanotransduction pathway.

While this study was under review, Chen et al. reported NMR and crystal structures of the SEAL domains from *H. thermocellum* RsgI1, RsgI2, and RsgI6 and the finding that these domains undergo

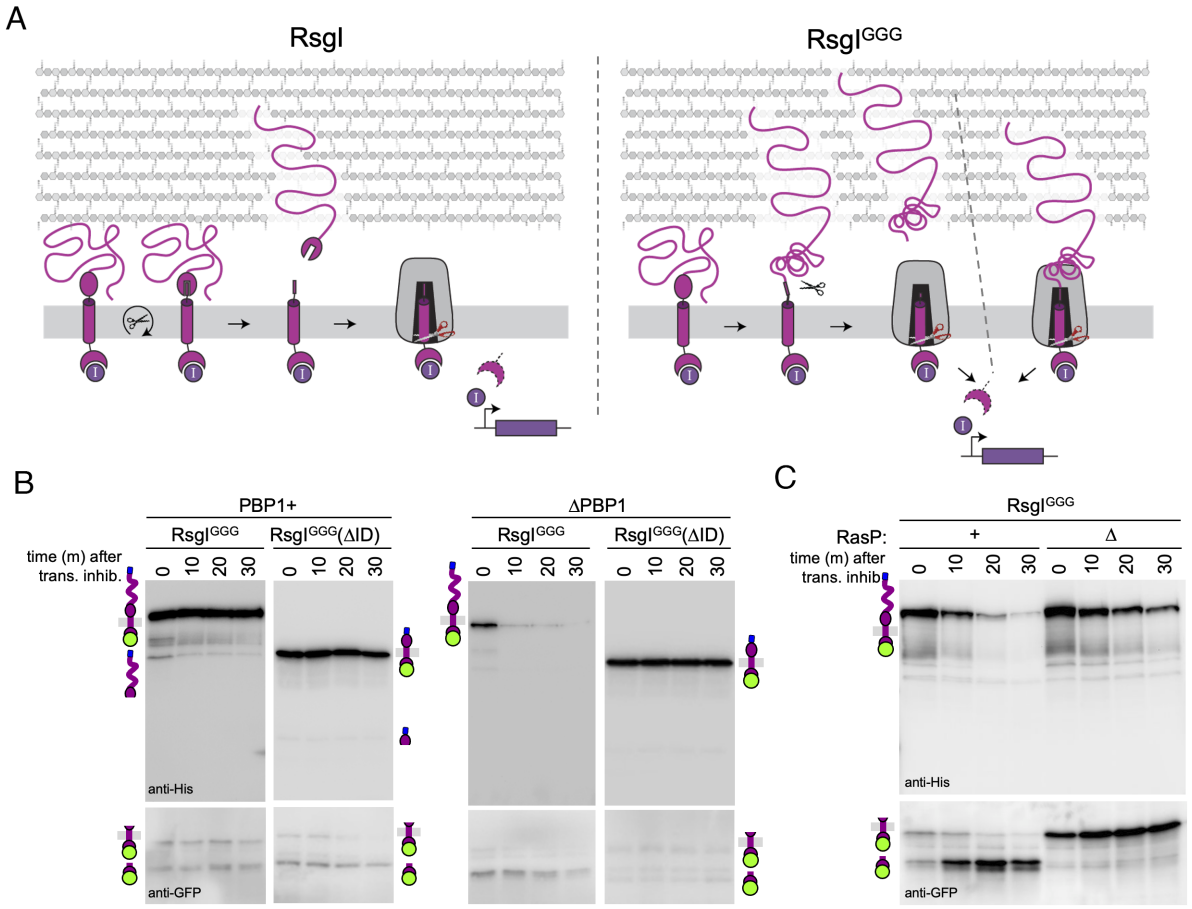

Fig. 6. RsgI's IDR is required to bypass site-1 autoproteolysis. (*A*) Schematic models of regulated intramembrane proteolysis of RsgI and the RsgI^{GGG} mutant. Detection of cell wall defects by RsgI's IDR generates a force that pulls the autoproteolyzed SEAL domain apart enabling RasP-mediated intramembrane proteolysis (*Left*). The same pulling force unfolds the uncleaved SEAL^{GGG} domain, which becomes susceptible to an extracytoplasmic protease and/or can access the recessed interior of the RasP protease (*Right*). (*B*) Immunoblots of strains constitutively expressing the indicated GFP-RsgI^{GGG}-His variants in the presence of absence of PBP1. Cells were harvested at the indicated times in minutes before and after inhibition of protein synthesis with chloramphenicol and spectinomycin. The intrinsically disordered region (ID) on RsgI^{GGG} is required to bypass autoproteolysis in the RIP signaling pathway. (*C*) Immunoblots of cells expressing GFP-RsgI^{GGG}-His in the presence or absence of RasP. Cells were harvested at the indicated times in minutes before and after addition of moenomycin to inhibit PBP1 and chloramphenicol and spectinomycin to inhibit protein synthesis. All immunoblots were performed in biological triplicate and representative blots are shown.

autoproteolysis, as we have described here (30). The structures of the cleaved *H. thermocellum* SEAL domains have a similar fold to *B. subtilis* RsgI^{GGG} and contain analogous extensions of the β-strands proximal to the cleavage site. Analysis of these RsgI homologs in vivo provides support for the regulation of intramembrane proteolysis similar to the one proposed here (4) (Fig. 3*A*). Interestingly, signal transduction was dampened in autoproteolysis-deficient mutants of RsgI6, in contrast to our findings for *B. subtils* RsgI. Collectively, their data support the model of mechanotransducive activation of RsgI homologs in Clostridial species and provide an example in which site-1 autoproteolysis is critical for signal transduction.

Bacterial SEAL Domains. SEAL domains are broadly conserved among Firmicutes but largely absent in other bacterial phyla (*SI Appendix*, Fig. S11). These domains are most often found in anti-sigma factors with a domain organization similar to *B. subtilis* RsgI. However, we identified many examples in which the anti-sigma factor had an additional domain appended to the IDR, as is found on *H. thermocellum* RsgIs (*SI Appendix*, Fig. S12). In total, we found seven distinct domains appended onto the IDR of RsgI-like anti-sigma factors that contain SEAL domains (*SI Appendix*, Table S3). In most cases, these domains are predicted to bind glycopolymers but others could bind extracellular proteins. In fact, the SEAL domain is frequently appended to PepSY domains, a poorly characterized domain that has been implicated in inhibiting extracellular enzymes (37). Interestingly, the SEAL–PepSY fusions lack an IDR and in some cases lack a cytoplasmic anti-sigma factor domain or even a TM segment. In virtually all cases, SEAL domain-containing proteins possess the highly conserved residues in the β-hairpin involved in catalysis. Biochemical analysis of SEAL domains from two distinct protein families revealed that both undergo autoproteolysis in *E. coli* and the cleavage products noncovalently interact (*SI Appendix*, Fig. S13). We hypothesize that most if not all SEAL domain-containing proteins autocleave yet remain associated. We further speculate that many of these proteins function in mechanotransduction.

Common Mechanisms of Mechanotransduction. The structure of bacterial SEAL domains is similar to eukaryotic SEA domains; however, the interconnectivity of the structural elements is distinct, arguing that these domains arose from convergent evolution. It is therefore particularly striking how similarly these domains are employed in signal transduction. The most well-studied SEA domain-containing protein, MUC1, highlights these similarities. MUC1 contains a cytoplasmic signaling domain, a single transmembrane helix, and an extracytoplasmic SEA domain followed by an extensive IDR (Fig. 7) (38). Both MUC1 and RsgI undergo constitutive autoproteolysis in their SEA/SEAL domains and their cleavage products remain noncovalently associated at the cell surface. Shear stress from pathogen binding to MUC1's heavily

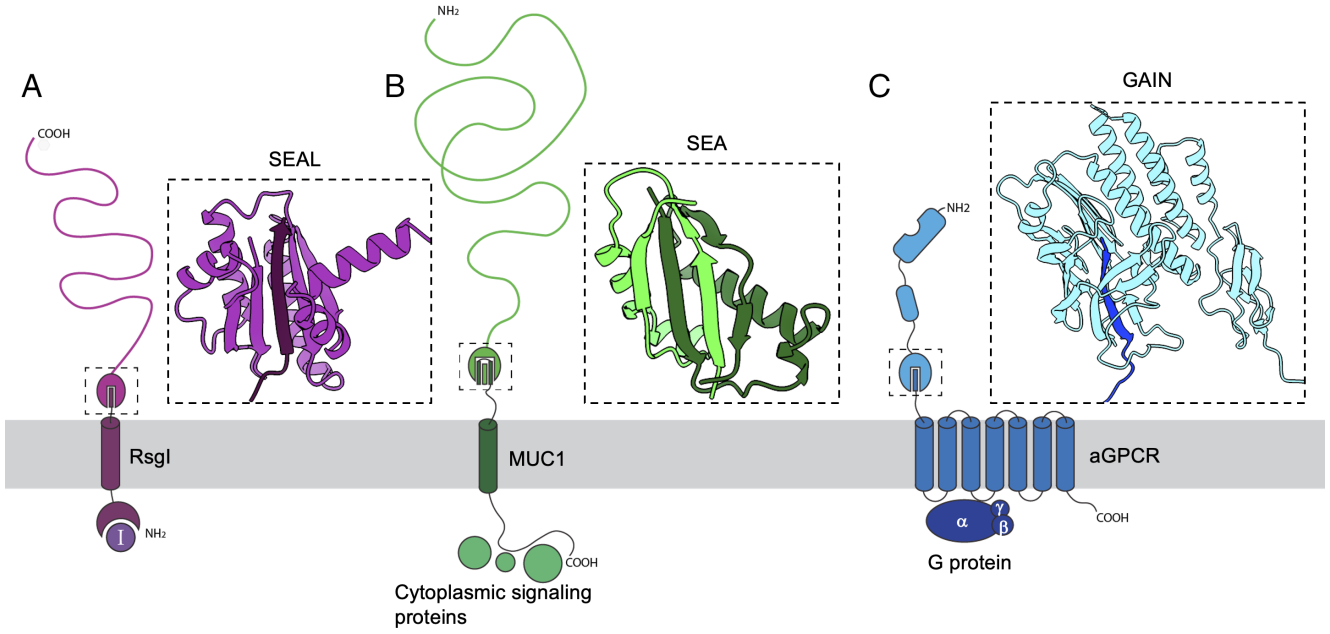

Fig. 7. A common feature of mechanotransducive pathways. Schematic models of RsgI, Mucin-1 (MUC1), and an adhesion G protein–coupled receptor (aGPCR). (*A*) RsgI undergoes autoproteolysis in its SEAL domain and the N (dark purple) and C-terminal (light purple) fragments remain noncovalently associated through an undisrupted β-sheet. (*B*) MUC1 undergoes autoproteolysis in its SEA domain (pdb: 6bsb) and the C- (dark green) and N-terminal (light green) fragments remain noncovalently associated. Each cleaved product contributes two strands to the undisrupted β-sheet. MUC1 has a large glycosylated extracellular intrinsically disordered region, and cytoplasmic signaling proteins associate with its intracellular domain. (*C*) aGPCRs are autoproteolyzed within their GAIN domain (pdb: 4dlq), and the C-terminal (dark blue) and N-terminal (light blue) fragments remain noncovalently associated through an undisrupted β-sheet. One or more extracellular adhesion domains are linked to the GAIN domain. The C-terminal strand of the GAIN domain is the tethered peptide agonist that, upon exposure, activates G-protein signaling.

glycosylated IDR has been implicated in dissociation of the N- and C-terminal fragments (39, 40). Although signaling through MUC1's cytoplasmic domain is less well understood, evidence suggests that MUC1 is subject to intramembrane proteolysis by gamma-secretase (41). Furthermore, translocation of the MUC1's free cytoplasmic domain to the cytoplasm, nucleus, and mitochondria has been documented (42). This signaling pathway requires further investigation but the work described here raises the exciting possibility that MUC1 could be regulated by a mechanotransduction pathway analogous to RsgI. Many other Mucins and cell surface proteins contain cytoplasmic signaling domains and extracytoplasmic SEA domains that undergo autoproteolysis suggesting that these proteins could similarly function in RIP signaling.

Unlike MUC1 signaling, adhesion GPCRs (aGPCRs) have been extensively characterized, and the similarities to RsgI signaling merit discussion. aGPCRs undergo autoproteolysis in a highly conserved extracytoplasmic domain called the GPCR Autoproteolysis INducing (GAIN) domain (18). This domain does not resemble SEA or SEAL domains. However, the GAIN domain cleavage products remain stably associated through a β-sheet network similar to SEA/SEAL domains (Fig. 7). Autoproteolysis occurs adjacent to the final β-strand that connects to the GPCR transmembrane domain, much like the autocleavage site in RsgI. This β-strand is termed the "tethered peptide" and functions as an agonist of aGPCR signaling (43, 44). The peptide is shielded from interacting with the GPCR transmembrane domain when it is embedded in the β-sheet network, but upon force imparted by the extracellular adhesion domains, the ectodomain is released exposing the peptide that, in turn, activates G Protein signaling (2). Interestingly, it has been shown that abolishing autocleavage in the GAIN domain is not sufficient to disrupt this signaling pathway (43, 45, 46). Recent structural data suggest that unfolding of the GAIN domain liberates the tethered peptide, which can still interact with the GPCR transmembrane domain without cleavage (46). Our data suggesting that unfolding the SEAL domain enables RasP-mediated intramembrane cleavage without ectodomain release shares striking parallels.

Our analysis of $RsgI^{GGG}$ also indicates that an unidentified extracytoplasmic protease can cleave the partially or fully unfolded SEAL domain. This cleavage allows the membrane-anchored portion of RsgI to more efficiently access the recessed interior of the membrane-embedded protease. We suspect that this alternate site-1 cleavage is not normally used in *B. subtilis* when RsgI autoproteolysis is intact. However, we hypothesize that RsgI homologs exist that are not proficient in autoproteolysis but could still leverage mechanotransduction using site-1 proteases that cleave partially or fully unfolded SEAL domains. This type of RIP signaling would be analogous to the Notch pathway in which endocytosis generates a pulling force that unfolds the negative regulatory region (NRR) of Notch, enabling site-1 cleavage by an ADAM family protease (47). We conclude by marveling at the strikingly similar mechanisms of mechanotransduction employed by bacteria and eukaryotes.

Methods

General Methods. All *B. subtilis* strains were derived from the prototrophic strain PY79 (48). Unless otherwise indicated, cells were grown in LB or defined rich (casein hydrolysate, CH) medium (49) at 37 °C. Insertion–deletion mutations were generated by isothermal assembly (50) of PCR products followed by direct transformation into *B. subtilis*. Tables of strains, plasmids, and oligonucleotide primers and a description of strain and plasmid construction can be found online as *SI Appendix* (*SI Appendix*, Tables S4–S7 and Plasmid Construction).

β-Galactosidase Assays. *B. subtilis* strains were grown in LB medium at 37 °C to an OD_{600} of ~0.7. The optical density was recorded and 1 mL of culture was harvested and assayed for β-galactosidase activity as previously described (51). Briefly, cell pellets were resuspended in 1 mL Z buffer (40 mM NaH_2PO_4, 60 mM Na_2HPO_4, 1 mM $MgSO_4$, 10 mM KCl, and 50 mM β-mercaptoethanol). Then, 250 µL of this suspension was added to 750 µL of Z buffer supplemented with

lysozyme (0.25 mg/mL), and the samples were incubated at 37 °C for 15 min. The colorimetric reaction was initiated by the addition of 200 μL of 2-nitrophe nyl-β-D-galactopyranoside (ONPG, 4 mg/mL) in Z buffer and stopped with 500 μL 1M Na_2CO_3. The reaction time and the absorbance at 420 nm and OD_{550} of the reactions were recorded, and the β-galactosidase-specific activity in Miller Units was calculated according to the formula $[A_{420}-1.75\times(OD_{550})]/(\text{time [min]} \times OD_{600}) \times \text{dilution factor} \times 1{,}000$ (52).

Immunoblot Analysis. Immunoblot analysis was performed as described previously (53). Briefly, 1 mL of culture was collected and resuspended in lysis buffer (20 mM Tris pH 7.0, 10 mM $MgCl_2$ and 1mM Ethylenediaminetetraacetic Acid (EDTA), 1 mg/mL lysozyme, 10 μg/mL DNase I, 100 μg/mL Rnase A, 1 mM PMSF) to a final OD_{600} of 10 for equivalent loading. The cells were incubated at 37 °C for 15 min followed by addition of an equal volume of Laemelli sample buffer (0.25 M Tris pH 6.8, 4% SDS, 20% glycerol, 10 mM EDTA) containing 10% β-mercaptoethanol. Samples were heated for 15 min at 65 °C prior to loading. Proteins were separated by SDS-PAGE on 12.5% polyacrylamide gels, electroblotted onto Immobilon-P membranes (Millipore), and blocked in 5% nonfat milk in phosphate-buffered saline (PBS) with 0.5% Tween-20. The blocked membranes were probed with anti-SigA (1:10,000) (54), anti-His (1:4,000) (GenScript), and anti-GFP (1:10,000) (55) antibodies diluted into 3% Bovine Serum Albumin (BSA) in PBS with 0.05% Tween-20. Primary antibodies were detected using horseradish peroxidase-conjugated goat anti-rabbit or anti-mouse IgG (BioRad) and the Super Signal chemiluminescence reagent as described by the manufacturer (Pierce). Signal was detected using a Bio-Techne FluorChem R System.

In Vivo Protein Turnover Assay. In vivo protein turnover assays were performed as previously described (4). In brief, *B. subtilis* strains were grown in LB medium at 37 °C to an OD_{600} of 0.5. Protein translation was inhibited by the addition of both spectinomycin (200 μg/mL, final concentration) and chloramphenicol (10 μg/mL, final concentration). Then, 1 mL samples normalized to an OD600 of 0.5 were collected immediately prior to antibiotic treatment and at the indicated times after. Cells were pelleted by centrifugation for 5 min and immediately flash-frozen in liquid nitrogen. The cell pellets were thawed on ice, lysed, and analyzed by immunoblot as described above.

Purification of His-Sumo-RsgI and Variants. Expression plasmids containing His-SUMO-RsgI variants were transformed into *E.coli* BL21(DE3) Δ*tonA* cells. Transformants were subcultured in terrific broth (TB) + 100 μg/mL ampicillin for 3 h and then back-diluted into 1 L TB + 100 μg/mL ampicillin to an OD600 of 0.01 and grown at 37 °C to an OD600 of 0.4. Cultures were induced with 500 μM IPTG for 3 h at 37 °C and then harvested by centrifugation at 4,000 rpm for 15 min. Pellets were resuspended in Lysis Buffer [50 mM HEPES-NaOH, 300 mM NaCl, 25 mM Imidazole, 10% (v/v) glycerol] and frozen at −80 °C. Cell pellets were thawed on ice and lysed by two passes through a cell disrupter at 25 kPsi. Then, 125 U Benzonase (Sigma) and 1X complete protease inhibitor (Roche) were added to the cell lysate and incubated on ice for 15 min. Lysates were clarified by ultracentrifugation at 40,000 rpm for 45 min at 4 °C. The supernatant was passed two times over a column with 500 μL of Ni^{2+}-NTA resin, washed with 50 bed volumes of wash buffer [20 mM HEPES-NaOH, 300 mM NaCl, 25 mM Imidazole, 10% (v/v) glycerol], and eluted in 5 mL of elution buffer [20 mM HEPES-NaOH, 300 mM NaCl, 300 mM Imidazole, 10% (v/v) glycerol].

When monitoring purified His-SUMO-RsgI variants for autoproteolysis, the protein concentration of each eluate was determined using a noninterfering protein concentration determination kit (G-Biosciences), and each prep was normalized to 1 mg/mL. Purified protein was placed at 37 °C, and at indicated times points, a sample was removed and mixed with an equal volume Laemelli SDS sample buffer containing 10% β-mercaptoethanol to stop the reaction. Samples were visualized by SDS-PAGE using 17.5% polyacrylamide gels and stained with Instant Blue (Abcam).

Size-Exclusion Chromatography. His-SUMO-SEAL and His-SUMO-$SEAL^{GGG}$ were analyzed by size-exclusion chromatography (SEC) on a Superdex S75 column (GE Healthcare) in buffer containing 20 mM of HEPES-NaOH, pH 7.5, and 300 mM of NaCl. The load and peak absorbance (A280) fractions were diluted into equal volume 2× sample buffer containing 10% β-mercaptoethanol and resolved by SDS-PAGE using a 17.5% polyacrylamide gel and stained with Instant Blue (Abcam). Absorbance profiles were plotted using MATLAB.

Edman Degradation and MALDI-TOF Analyses. Following purification of His-SUMO-RsgI homologs, the eluates were treated with 6.25 μg of Ulp1 and dialyzed at 4 °C overnight in Dialysis Buffer (20 mM HEPES-NaOH, 300 mM NaCl, 10% glycerol) with a 3kDa Molecular Weight Cutoff (MWCO). The sample was loaded onto a BioRad column containing 500 μL of Ni-NTA resin and passed three times over the resin before the flowthrough containing purified RsgI variant was collected. The buffer was exchanged into water using a 3 kDa ultracentrifugal filter (Sigma) and the protein was analyzed by MALDI-TOF using an Applied Biosystems Voyager DE Pro in linear mode (Tufts University Core Facility).

Purified SEAL variants as described above were separated by SDS-PAGE using 17.5% polyacrylamide gels and transferred to a PVDF membrane at 90 V for 60 min. The membrane was then washed 5× with ddH_2O, stained with 0.02% Coomassie Brilliant blue in 40% methanol, 5% acetic acid for 30 s, destained in 40% methanol, 5% acetic acid for 1 min, washed 3× with ddH_2O, and allowed to air dry. The bands of interest were cut from the membrane and sent for five cycles of Edman Degradation analysis with an ABI 494 Protein Sequencer (Tufts University Core Facility).

In Vitro Transcription–Translation Reactions. In vitro transcription–translation reactions were carried out using the NEB PURExpress system and its published protocol (https://www.neb.com/protocols/0001/01/01/protein-synthesis-reaction-using-purexpress-e6800). Briefly, Solution A, Solution B, and ^{35}S-methionine were combined with 250 ng pAB87, pAB101, or pDHFR as a positive control. The reactions were incubated for 1 h at 37 °C, and 5 μL of the reaction was combined with equal volume Laemalli Sample Buffer containing 10% β-mercaptoethanol to stop the reaction. Chloramphenicol (25 μg/mL final) was added to the transcript–translation reaction after 60 min, to inhibit protein synthesis and samples were mixed with Laemelli Sample buffer at the indicated times. Proteins were separated by SDS-PAGE using a 17.5% polyacrylamide gel, the gel was dried, exposed to a phosphor screen, and imaged with an Amersham Typhoon IP (Cytiva). Samples were also visualized by immunoblot using anti-GFP antibodies as described above.

$RsgI^{GGG}$ Purification for Crystallography. pAB188 [His-Sumo-$SEAL^{GGG}$] was transformed into BL21(DE3) Δ*tonA* cells. Transformants were subcultured in terrific broth (TB) with 100 μg/mL ampicillin at 37 °C for 3 h then back-diluted into 3 L TB + 100 μg/mL ampicillin to an OD600 of 0.01 and grown at 37 °C to an OD600 of 0.4. Cultures were induced with 500 μM IPTG for 3 h before collection by centrifugation at 4,000 rpm. Pellets were resuspended in Lysis Buffer (50 mM HEPES-KOH pH 7.5, 250 mM NaCl, 25 mM Imidazole, 10% v/v glycerol) and frozen at −80 °C. Cell pellets were thawed on ice and lysed by two passes through a cell disrupter at 25k Psi. Then, 125 U Benzonase (Sigma) and 1X complete protease inhibitor (Roche) were added to the cell lysate and incubated on ice for 15 min. Lysates were clarified by ultracentrifugation at 40,000 rpm for 45 min at 4 °C. The supernatant was passed two times over a column with 1.5 mL of Ni^{2+}-NTA resin (Qiagen), washed with 50 bed volumes of wash buffer [20 mM HEPES-KOH, 250 mM NaCl, 25 mM Imidazole, 10% (v/v) glycerol], and eluted in 10 mL of elution buffer [20 mM HEPES-KOH, 250 mM NaCl, 300 mM Imidazole, 10% (v/v) glycerol]. Then, 6.25 μg of Ulp1 was added to the eluate to remove the His-SUMO tag and was dialyzed (3 kDa MWCO) overnight at 4 °C in dialysis buffer (20 mM HEPES-KOH, 250 mM NaCl, 10% v/v glycerol, 1 mM TCEP). The dialyzed elution was passed over a column containing 1.5 mL of Ni^{2+}-NTA resin three times and the flowthrough was collected and analyzed for purity by SDS-PAGE. The $SEAL^{GGG}$ domain was purified by size exclusion chromatography (SEC) on a Superdex S75 column (GE Healthcare) in buffer containing 20 mM of HEPES-KOH pH 7.5, 250 mM of NaCl, and 1 mM TCEP. The peak absorbance (A280) fraction was collected and concentrated to 22 mg/mL using a 3 kDa MWCO concentrator (Millipore) before flash-freezing in liquid nitrogen.

Crystallization and Structure Determination. $RsgI^{GGG}$ was crystallized using the hanging drop vapor diffusion method at 18 °C. Native protein was thawed on ice and diluted into a buffer solution (20 mM HEPES-KOH pH 7.5, 20 mM NaCl, 1 mM TCEP) to a final concentration of 8 mg/mL. Crystals were grown by mixing 1 μL of purified protein with 1 μL of a reservoir solution of 100 mM HEPES-KOH pH 7.5, 100 mM ammonium acetate, and 28% PEG-3350 (w/v) in EasyXtal 15-well trays (NeXtal) containing 400 μL reservoir solution. $RsgI^{GGG}$ crystallized over 7 d and crystals were harvested and cryoprotected in reservoir solution supplemented with 15% ethylene glycol before freezing in liquid nitrogen.

X-ray diffraction data were collected at the Advanced Photon Source (beamline 24-ID-C) and data were processed using the SSRL autoxds script (A. Gonzalez, Stanford SSRL). An AlphaFold2 model of RsgI^{GGG} was used for molecular replacement to determine phase information and an initial map was determined using the Phaser program in Phenix v1.20.1 (56). Statistics were analyzed as described in *SI Appendix*, Table S2. Model building was performed in Coot (57) and refinement was performed using Phenix. The structures are deposited in the Protein Data Bank (PDB) under code 8T9N.

Bioinformatics Analysis. A local pblast run was performed on the amino acid sequence of *B.subtilis* RsgI's SEAL domain against the RefSeq select database using an e-value cutoff of 0.05. The resulting scientific names were converted to taxids using NCBI's taxid identifier (https://www.ncbi.nlm.nih.gov/Taxonomy/TaxIdentifier/tax_identifier.cgi) (58) and taxids were used to plot onto a phylogenetic tree of 5767 unique bacterial taxa. The tree was constructed using iTOL (https://itol.embl.de/) (59).

The resulting FASTA files from the pblast search were annotated using local PfamScan (60) (https://www.ebi.ac.uk/seqdb/confluence/display/THD/PfamScan) against the Pfam database. The output domains were organized based on Refseq accession number and the resulting domain organizations built. Counts of each domains identified can be found in *SI Appendix* (*SI Appendix*, Table S3).

Multiple Sequence Alignment. Multiple sequence alignments were generated using Clustal Omega (https://www.ebi.ac.uk/Tools/msa/clustalo/) (60).

Alphafold2 Predictions. Protein structures were modeled using AlphaFold2 (21) and ColabFold run using the Alphafold2 Advanced Colab notebook (61) (https://colab.research.google.com/github/sokrypton/ColabFold/blob/main/beta/AlphaFold2_advanced.ipynb) or downloaded (A0A6M4JFI2, A3DC27, A3DCG3, and A0A1V4I8Y9) from the Alphafold database (62) (available at: https://alphafold.ebi.ac.uk/). The parameters for the run were as follows: msa method mmseq2, pair mode unpaired, maximum recycling 3, no templates, five models generated. The highest ranked structure by pLDDT is shown.

Structural Model Visualization. Crystal structures of MUC1 (pdb: 6bsb) and aGPCR (pdb: 4dlq) were downloaded from the PDB. ChimeraX1.3 and Pymol 2.4.0 were used to visualize the structural models and generate images. PDBsum was used to generate MUC1 SEA and RsgI SEAL protein topology maps (63).

Data, Materials, and Software Availability. Raw data for all graphs has been uploaded as source data. Uncropped immunoblots and SDS-PAGE gels are included in the *SI Appendix*. Plasmids, primers, synthetic DNA constructs and strains used can be found in *SI Appendix*, Tables S1–S7. The X-ray crystal structure of the SEAL^{GGG} domain has been deposited in the Protein Data Bank (available at: https://www.rcsb.org/) with accession code 8T9N (64).

ACKNOWLEDGMENTS. We thank all members of the Bernhardt-Rudner supergroup for helpful advice, discussions, and encouragement, Kailey Slavik, Yao Li, and the Kranzusch lab for help with in vitro transcription–translation reactions, crystallization trials, and structure determination, Lior Artzi for Clostridial genomic DNAs, Suzanne Walker for moenomycin A, the Tufts University Core Facility (TUCF) and Taplin Biological Mass Spectrometry Facility for proteomic analysis, and Ernst Schmid for help with analysis of Alphafold2 predictions. Portions of this research were conducted on the O2 High Performance Computing Cluster, which is supported by the Research Computing Group at Harvard Medical School. Support for this work comes from the NIH Grants R35GM145299 and U19 AI158028 (D.Z.R.). A.P.B. was funded in part by NSF (DGE1745303).

Author affiliations: [a]Department of Microbiology, Harvard Medical School, Boston, MA 02115; and [b]Department of Cancer Immunology and Virology, Dana-Farber Cancer Institute, Boston, MA 02115

1. T. Langenhan, Adhesion G protein–coupled receptors–Candidate metabotropic mechanosensors and novel drug targets. *Basic Clin. Pharmacol. Toxicol.* **126**, 5–16 (2020).
2. A. Vizurraga, R. Adhikari, J. Yeung, M. Yu, G. G. Tall, Mechanisms of adhesion G protein–coupled receptor activation. *J. Biol. Chem.* **295**, 14065–14083 (2020).
3. D. Sprinzak, S. C. Blacklow, Biophysics of notch signaling. *Annu. Rev. Biophys.* **50**, 157–189 (2021).
4. Y. R. Brunet, C. Habib, A. P. Brogan, L. Artzi, D. Z. Rudner, Intrinsically disordered protein regions are required for cell wall homeostasis in *Bacillus subtilis*. *Genes Dev.* **36**, 970–984 (2022).
5. M. S. Brown, J. Ye, R. B. Rawson, J. L. Goldstein, Regulated intramembrane proteolysis A control mechanism conserved from bacteria to humans. *Cell* **100**, 391–398 (2000).
6. J. Heinrich, T. Wiegert, Regulated intramembrane proteolysis in the control of extracytoplasmic function sigma factors. *Res. Microbiol.* **160**, 696–703 (2009).
7. Y. Hizukuri *et al.*, A structure-based model of substrate discrimination by a noncanonical PDZ tandem in the intramembrane-cleaving protease RseP. *Structure* **22**, 326–336 (2014).
8. K. Akiyama *et al.*, Roles of the membrane-reentrant β-hairpin-like loop of RseP protease in selective substrate cleavage. *eLife* **4**, e08928 (2015).
9. Y. Patel, H. Zhao, J. D. Helmann, A regulatory pathway that selectively up-regulates elongasome function in the absence of class A PBPs. *eLife* **9**, e57902 (2020).
10. C.-L. Tseng, J.-T. Chen, J.-H. Lin, W.-Z. Huang, G.-C. Shaw, Genetic evidence for involvement of the alternative sigma factor SigI in controlling expression of the cell wall hydrolase gene lytE and contribution of LytE to heat survival of Bacillus subtilis. *Arch. Microbiol.* **193**, 677 (2011).
11. L. I. Salzberg *et al.*, The WalRK (YycFG) and sI RsgI regulators cooperate to control CwlO and LytE expression in exponentially growing and stressed Bacillus subtilis cells. *Mol. Microbiol.* **87**, 180–195 (2013).
12. C.-L. Tseng, G.-C. Shaw, Genetic evidence for the actin homolog gene mreBH and the bacitracin resistance gene bcrC as targets of the alternative sigma factor Sigi of *Bacillus subtilis*. *J. Bacteriol.* **190**, 1561–1567 (2008).
13. P. Bork, L. Patthy, The SEA module: A new extracellular domain associated with O-glycosylation. *Protein Sci.* **4**, 1421–1425 (1995).
14. F. Levitin *et al.*, The MUC1 SEA module is a self-cleaving domain*. *J. Biol. Chem.* **280**, 33374–33386 (2005).
15. B. Macao, D. G. A. Johansson, G. C. Hansson, T. Härd, Autoproteolysis coupled to protein folding in the SEA domain of the membrane-bound MUC1 mucin. *Nat. Struct. Mol. Biol.* **13**, 71–76 (2006).
16. T. Pelaseyed *et al.*, Unfolding dynamics of the mucin SEA domain probed by force spectroscopy suggest that it acts as a cell-protective device. *FEBS J.* **280**, 1491–1501 (2013).
17. J. Pei, N. V. Grishin, Expansion of divergent SEA domains in cell surface proteins and nucleoporin 54. *Protein Sci.* **26**, 617–630 (2017).
18. D. Araç *et al.*, A novel evolutionarily conserved domain of cell-adhesion GPCRs mediates autoproteolysis. *EMBO J.* **31**, 1364–1378 (2012).
19. A. Sandberg, D. G. A. Johansson, B. Macao, T. Härd, SEA domain autoproteolysis accelerated by conformational strain: Energetic aspects. *J. Mol. Biol.* **377**, 1117–1129 (2008).
20. D. G. A. Johansson, B. Macao, A. Sandberg, T. Härd, SEA domain autoproteolysis accelerated by conformational strain: Mechanistic aspects. *J. Mol. Biol.* **377**, 1130–1143 (2008).
21. J. Jumper *et al.*, Highly accurate protein structure prediction with AlphaFold. *Nature* **596**, 583–589 (2021).
22. L. Holm, Dali server: Structural unification of protein families. *Nucleic Acids Res.* **50**, gkac387 (2022).
23. M. E. Noguera, J. Jakoncic, M. R. Ermácora, High-resolution structure of intramolecularly proteolyzed human mucin-1 SEA domain. *Biochim. Biophys. Acta (BBA) - Proteins Proteom.* **1868**, 140361 (2020).
24. Y. Zhang, J. Skolnick, TM-align: A protein structure alignment algorithm based on the TM-score. *Nucleic Acids Res.* **33**, 2302–2309 (2005).
25. M. J. Ligtenberg *et al.*, Cell-associated episialin is a complex containing two proteins derived from a common precursor. *J. Biol. Chem.* **267**, 6171–6177 (1992).
26. H. Kahel-Raifer *et al.*, The unique set of putative membrane-associated anti-σ factors in Clostridium thermocellum suggests a novel extracellular carbohydrate-sensing mechanism involved in gene regulation. *FEMS Microbiol. Lett.* **308**, 84–93 (2010).
27. Y. Nataf *et al.*, Clostridium thermocellum cellulosomal genes are regulated by extracytoplasmic polysaccharides via alternative sigma factors. *Proc. Natl. Acad. Sci. U.S.A.* **107**, 18646–18651 (2010).
28. L. O. de Ora *et al.*, Regulation of biomass degradation by alternative σ factors in cellulolytic clostridia. *Sci. Rep.* **8**, 11036 (2018).
29. I. Muñoz-Gutiérrez *et al.*, Decoding biomass-sensing regulons of Clostridium thermocellum alternative Sigma-I factors in a heterologous Bacillus subtilis host system. *PLoS One* **11**, e0146316 (2016).
30. C. Chen *et al.*, Essential autoproteolysis of bacterial anti-σ factor RsgI for transmembrane signal transduction. *Sci. Adv.* **9**, eadg4846 (2023).
31. S. Parry *et al.*, Identification of MUC1 proteolytic cleavage sites in vivo. *Biochem. Biophys. Res. Commun.* **283**, 715–720 (2001).
32. T. Palmai-Pallag *et al.*, The role of the SEA (sea urchin sperm protein, enterokinase and agrin) module in cleavage of membrane-tethered mucins. *FEBS J.* **272**, 2901–2911 (2005).
33. D. G. A. Johansson *et al.*, Protein autoproteolysis: Conformational strain linked to the rate of peptide cleavage by the pH dependence of the N → O acyl shift reaction. *J. Am. Chem. Soc.* **131**, 9475–9477 (2009).
34. J. van Heijenoort, Formation of the glycan chains in the synthesis of bacterial peptidoglycan. *Glycobiology* **11**, 25R–36R (2001).
35. W. R. Gordon *et al.*, Structural basis for autoinhibition of Notch. *Nat. Struct. Mol. Biol.* **14**, 295–300 (2007).
36. T.-Y. Liu, S.-H. Chu, Y.-N. Hu, J.-J. Wang, G.-C. Shaw, Genetic evidence that multiple proteases are involved in modulation of heat-induced activation of the sigma factor SigI in Bacillus subtilis. *FEMS Microbiol. Lett.* **364**, fnx054 (2017).
37. C. Yeats, N. D. Rawlings, A. Bateman, The PepSY domain: A regulator of peptidase activity in the microbial environment? *Trends Biochem. Sci.* **29**, 169–172 (2004).
38. C. L. Hattrup, S. J. Gendler, Structure and function of the cell surface (tethered) mucins. *Annu. Rev. Physiol.* **70**, 431–457 (2008).
39. K. C. Kim, Role of epithelial mucins during airway infection. *Pulm. Pharmacol. Ther.* **25**, 415–419 (2012).
40. J. P. M. van Putten, K. Strijbis, Transmembrane mucins: Signaling receptors at the intersection of inflammation and cancer. *J. Innate Immun.* **9**, 281–299 (2017).
41. J. Julian, N. Dharmaraj, D. D. Carson, MUC1 is a substrate for γ-secretase. *J. Cell. Biochem.* **108**, 802–815 (2009).
42. D. D. Carson, The cytoplasmic tail of MUC1: A very busy place. *Sci. Signal.* **1**, pe35 (2008).
43. I. Liebscher *et al.*, A tethered agonist within the ectodomain activates the adhesion G protein–coupled receptors GPR126 and GPR133. *Cell Rep.* **9**, 2018–2026 (2014).

44. H. M. Stoveken, A. G. Hajduczok, L. Xu, G. G. Tall, Adhesion G protein-coupled receptors are activated by exposure of a cryptic tethered agonist. *Proc. Natl. Acad. Sci. U.S.A.* **112**, 6194–6199 (2015).
45. S. Prömel *et al.*, The GPS motif is a molecular switch for bimodal activities of adhesion class G protein-coupled receptors. *Cell Rep.* **2**, 321–331 (2012).
46. X. Qu *et al.*, Structural basis of tethered agonism of the adhesion GPCRs ADGRD1 and ADGRF1. *Nature* **604**, 779–785 (2022).
47. W. R. Gordon *et al.*, Mechanical allostery: Evidence for a force requirement in the proteolytic activation of notch. *Dev. Cell* **33**, 729–736 (2015).
48. P. J. Youngman, J. B. Perkins, R. Losick, Genetic transposition and insertional mutagenesis in Bacillus subtilis with Streptococcus faecalis transposon Tn917. *Proc. Natl. Acad. Sci. U.S.A.* **80**, 2305–2309 (1983).
49. C. R. Harwood, S. M. Cutting, *Molecular Biological Methods for Bacillus* (Wiley, 1990).
50. D. G. Gibson *et al.*, Enzymatic assembly of DNA molecules up to several hundred kilobases. *Nat. Methods* **6**, 343–345 (2009).
51. D. Z. Rudner, P. Fawcett, R. Losick, A family of membrane-embedded metalloproteases involved in regulated proteolysis of membrane-associated transcription factors. *Proc. Natl. Acad. Sci. U.S.A.* **96**, 14765–14770 (1999).
52. J. H. Miller, *Experiments in Molecular Genetics* (Cold Spring Harbor Laboratory, 1972).
53. X. Wang *et al.*, Condensin promotes the juxtaposition of DNA flanking its loading site in Bacillus subtilis. *Genes Dev.* **29**, 1661–1675 (2015).
54. M. Fujita, Y. Sadaie, Promoter selectivity of the Bacillus subtilis RNA polymerase 6k and CTH holoenzyme. *J. Biochem.* **124**, 89–97 (1998).
55. D. Z. Rudner, R. Losick, A sporulation membrane protein tethers the pro-σK processing enzyme to its inhibitor and dictates its subcellular localization. *Genes Dev.* **16**, 1007–1018 (2002).
56. D. Liebschner *et al.*, Macromolecular structure determination using X-rays, neutrons and electrons: Recent developments in Phenix. *Acta Crystallogr. Sect. D* **75**, 861–877 (2019).
57. P. Emsley, K. Cowtan, Coot: Model-building tools for molecular graphics. *Acta Crystallogr. Sect. D* **60**, 2126–2132 (2004).
58. E. W. Sayers *et al.*, Database resources of the national center for biotechnology information. *Nucleic Acids Res.* **50**, D20–D26 (2021).
59. I. Letunic, P. Bork, Interactive Tree Of Life (iTOL) v5: An online tool for phylogenetic tree display and annotation. *Nucleic Acids Res.* **49**, gkab301- (2021).
60. F. Madeira *et al.*, Search and sequence analysis tools services from EMBL-EBI in 2022. *Nucleic Acids Res.* **50**, W276–W279 (2022).
61. M. Mirdita *et al.*, ColabFold: Making protein folding accessible to all. *Nat. Methods* **19**, 679–682 (2022).
62. M. Varadi *et al.*, AlphaFold Protein Structure Database: Massively expanding the structural coverage of protein-sequence space with high-accuracy models. *Nucleic Acids Res.* **50**, D439–D444 (2021).
63. R. A. Laskowski, J. Jabłońska, L. Pravda, R. S. Vařeková, J. M. Thornton, PDBsum: Structural summaries of PDB entries. *Protein Sci.* **27**, 129–134 (2018).
64. A. P. Brogan, C. Habib, S. J. Hobbs, P. J. Kranzusch, D. Z. Rudner, 8T9N. Protein Data Bank. https://www.rcsb.org/structure/8T9N. Deposited 24 June 2023.